PCCP

Accepted Manuscript




ROYAL SOCIETY OF CHEMISTRY

www.rsc.org/pccp

Physical Chemistry Chemical Physics

Dynamic Article Links ►

Cite this: DOI: 10.1039/c0xx00000x

ARTICLE

www.rsc.org/xxxxxx

# Enhanced photocatalytic performance at Au/N-$TiO_2$ hollow nanowire array by combinatorial light scattering and reduced recombination

**P. Sudhagar,[a,c] Anitha Devadoss,[b,c‡] Taeseup Song,[b‡] P. Lakshmipathiraj,[c] Hyungkyu Han,[b] Volodymyr V. Lysak,[d] C. Terashima,[c] Kazuya Nakata,[c] A. Fujishima,[c] Ungyu Paik,[a,b]* and Yong Soo Kang [a]***

***Received (in XXX, XXX) Xth XXXXXXXXX 20XX, Accepted Xth XXXXXXXXX 20XX***
**DOI: 10.1039/b000000x**

We demonstrate one-step gold nanoparticles (AuNPs) coating and the surface nitridation on $TiO_2$ nanowires ($TiO_2$-NWs) to amplify the light photon reflection. The surface nitridation on $TiO_2$-NWs array maximizes the AuNPs anchoring and the subsequent band gap reduction from 3.26 eV to 2.69 eV affords visible light activity. The finite-difference time-domain method (FDTD) simulation clearly exhibits the enhancement in the strengths of localized electric field between AuNPs and NWs, which significantly improves the photocatalytic (PC) performance. Both nitridation treatment and AuNPs decoration on $TiO_2$-NWs result in beneficial effects in high ($e^-/h^+$) pair separation through healing of the oxygen vacancies. The combinatorial effect of visible light harvesting photons and reduced recombination in Au/N-doped $TiO_2$-NWs, unprecedentedly, promotes the photocatalytic activity towards degradation of methyl orange ~4 fold ($1.1 \times 10^{-2}$ min) higher than $TiO_2$-NWs ($2.9 \times 10^{-3}$ $min^{-1}$). The proposed AuNPs decoration on nitrated $TiO_2$-NWs surface can be transformed to wide range of n-type metal oxides for photoanodes in photocatalytic applications.

## Introduction

The seminal report on photosynthetic oxidation of water by Fujishima and Honda[1] opened a new paradigm in researching artificial photosynthesis for energy conversion solar fuel cells,[2-4] photocatalytic biosensors,[5, 6] carbon dioxide reduction,[7] self-cleaning coatings[8] and organic pollutant removal[9]. The merits in recovering and recycling the semiconductor photocatalytic electrodes are more viable and economic compared to suspended photocatalyst in environmental water purification application. In this line, simultaneous energy conversion (collection of photoelectrons) from photocatalytic electrodes during organic dye pollutant removal process is a land-mark advent, which provides the futuristic platform to obtaining useful carbon fuels from hazardous pollutant treatment.[10, 11] Particularly, solar light driven photocatalytic substances find great deal of attention for achieving renewable and low-cost organic pollutant treatment.

The semiconductor photocatalytic substance generates photocarriers (electrons and holes) under light irradiation (band gap illumination). The resultant photoholes at valence band (VB) form OH radicals, which further degrade the target pollutant components through a series of radical reactions. Whereas, the photoelectrons at conduction band (CB) gets converted into either $O_2$ radical in the pollutant medium or may be collected through the external circuit for useful fuel generation.[12] In general, the photocatalytic performance at pollutant removal relies on several factors such as substantial charge separation, electrode stability against photocorrosion, and more importantly the light photons harvesting at solar visible spectrum for solar driven photocatalytic performance.

Among the variety of photocatalysts, titanium dioxide ($TiO_2$) nanostructures incited considerable attention in the field of photocatalytic decolourization of organic pollutants owing to their chemical stability and substantial photocatalytic response. The VB position of $TiO_2$ (~3.0-3.2 eV NHE) is far from the water oxidation potential (1.2 eV NHE), which offers more energetic pathways in forming OH radicals, an indispensable parameter for organic dye pollutant degradation. However, the minimal access of visible light due to its intrinsic wide band gap 3.2 eV (absorbs only 3-5% of solar light photons) and the high rates of electron-hole pair recombination at surface states limit the photocatalytic efficiency.[13] A wide range of research has been devoted to promote the visible light photocatalytic activity of $TiO_2$ through minimized charge recombination via doping and decorating co-photocatalysts. In the case of doping strategy, metal ions (Fe, Cr, Cu)[14,15,16,17], metal clusters (Fe (III) and Cu (II))[18, 19], non-metallic elements (N,S and C)[20,21,22] and inducing defects in crystallite lattice[23, 24] at $TiO_2$ had shown efficient result in extending visible light performance. Primarily, these doping carries introduce the sub-bands above the valence band (VB) of $TiO_2$ (band gap narrowing) that could facilitate the visible light activity below 3.2

eV band gap energy. Alternatively, amplifying the light photons reception at $TiO_2$ by light scattering mechanism would be a prominent alternative to improve the activity without altering the electronic structure of $TiO_2$. Utilizing 1-D nanostructures such as nanowire, nanofibers and nanotubes etc., are of interest in promoting light scattering behaviour at electrode geometry owing to the multiple photons scattering in between 1-D channels; thus, retarding the light attenuation at the electrode.[25, 26] The efficient charge transport through 1-D geometry supports the electron supply to the donor counter parts compared to nanoparticulate architecture.

In addition to 1-D nanostructures, plasmonic nanoparticles (NPs) also exhibits strong light scattering property due to localized surface plasmon resonance (LSPR), which originates from collective oscillation of surface electrons.[27, 28] Several plasmonic photocatalysts were tested in photocatalytic decolourization of dyes and realized their substantial stability in the aqueous medium. [29-31] It is found that AuNPs can effectively promote the organic pollutant degradation rate of $TiO_2$ by inhibiting the recombination of photogenerated electron-hole pairs.[32, 33] It is anticipated that decorating AuNPs onto $TiO_2$ surface as an antenna produces light scattering that could effectively promote the light photons at near-UV band, which perhaps enhances the $TiO_2$ absorption in the same region.[28, 34] Thus, decorating $TiO_2$ nanostructures with light scattering plasmonic nanoparticles has opened a new means of improving the light absorption activity of $TiO_2$ in visible light region to improve the photocatalytic efficiency.[35, 36]

Though successful immobilization of AuNPs on oxide surfaces has been demonstrated previously[37, 38] they generally suffer from monodispersity, owing to the direct reduction of metal salts on $TiO_2$, and on the other hand, maintaining the stability and functionality of the hybrid materials remain challenging due to the adverse changes in the chemical environment of the oxide support. Particularly, there are no reports on facile one-step assembly of AuNPs onto metal oxide surface. Thus, formulating a straightforward method to assemble stable AuNPs on oxide surfaces seems imperative. Herein, we report a trouble-free one-step assembly technique for immobilizing AuNPs on one-dimensional N-doped $TiO_2$ nanowires (N-$TiO_2$-NWs). We found that the Au/N-$TiO_2$-NWs exhibit excellent catalytic activity towards photocatalytic decolourization of methyl orange (MO). Furthermore, the synergistic effect of N-doping and localized light scattering centres of AuNPs on the photocatalytic dye degradation were elucidated.

## Results and discussion

The crystallite phase of pristine and nitridated $TiO_2$-NWs were studied using X-ray diffraction spectra (See supporting information Fig. S1). The $TiO_2$-NWs show anatase phase and no rutile phase was observed. The monolayer protected AuNPs with 4-Dimethylaminopyridine (DMAP) were synthesized using a facile phase transfer protocol (See Experimental section). Fig.1a-d shows the electron microscopic images of AuNPs, N-$TiO_2$-NWs, Au/$TiO_2$-NWs and Au/N-$TiO_2$-NWs electrodes, respectively. Colloidal AuNPs exhibit superior monodispersity with a mean diameter of 4.5±0.5 nm (Fig.1a). The electrophoretic mobility measurements on AuNPs yielded an average ζ-potential of +17.3 mV, which arises from the partial protonation of the exocyclic nitrogen that extend away from the NPs surface toward the solvent. Fig. 1b shows the vertically aligned N-$TiO_2$-NWs. The vertically aligned $TiO_2$-NWs and N-$TiO_2$-NWs have a mean diameter of ~200 nm. Comparing Fig.1 (c) and (d), it is found that the $TiO_2$-NWs (Fig.1c) surface shows lower distribution of immobilized AuNPs than N-$TiO_2$-NWs (Fig.1d). This may be ascribed to the high affinity of DMAP functionalized Au towards nitrogen atom. It is reported that the isoelectric point (ISP) of $TiO_2$ surface turned from positive (zeta potential ~15.5 at pH 5.5) to highly negative by nitrogen doping (zeta potential -49.9 at pH 5.5).[39] This implies that highly negative ISP value of N-$TiO_2$ surface allows more positively polarized Au NPs decoration. The surface doping of N carriers at $TiO_2$-NWs is confirmed by X-ray photoelectron spectroscopy (See supporting information S2). Graciani et al. demonstrated that the surface adhesion energy of Au nanoparticles on $TiO_2$ surface has promoted the nitrogen implantation through improving the electron transfer from the Au 6s levels toward the N 2p levels.[40] Similarly, plasma nitridation (Fig.1d) on $TiO_2$ facilitated the interaction between $TiO_2$ and AuNPs. Further the high magnification TEM image of Au/N-$TiO_2$-NW and the elemental mapping confirms the existence of individual elements (Fig.1f) (also see supporting information Fig. S3 for clear visibility of elemental mapping).

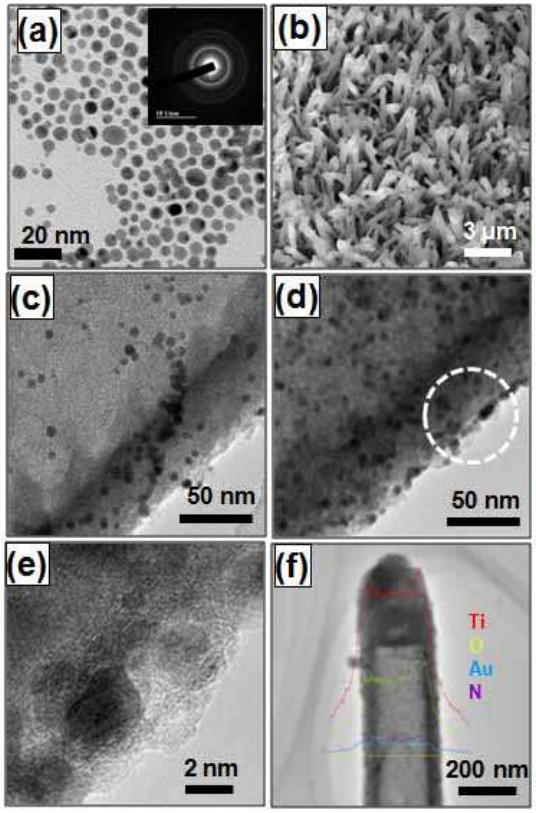


**Figure 1:** Electron microscope images of (a) DMAP-protected colloidal AuNPs (inset: selected area diffraction pattern), (b) N-$TiO_2$-NWs array, (c) Au/$TiO_2$-NWs and (d) Au/N-$TiO_2$-NWs. (e) and (f) shows the high magnification and elemental mapping of Au/N-$TiO_2$-NWs, respectively.

Figure 2 (a) shows the optical absorbance of $TiO_2$-NWs and N-$TiO_2$-NWs before and after decorating with AuNPs, which

implies that N-doping has shifted the absorbance edge of $TiO_2$ from UV to visible light wavelength due to the occupancy of N-ions in sub-surface states of $TiO_2$. This forms a sub-band gap above the valence band of $TiO_2$ and thus, facilitates the visible light activity.[41] The optical density (OD) of the pure and modified $TiO_2$ electrodes has been estimated as $F(R)^{1/2} = [(1-R^2)/2R]^{1/2}$ in Kubelka-Munk units (Fig.2b).[42] The optical density of $TiO_2$ is markedly enhanced at UV as well as visible light wavelength region owing to band gap narrowing and light reflection by N-doping and AuNPs decoration, respectively. Further in order to ensure the band gap narrowing effect at N-$TiO_2$ NWs, the valence band maximum position was estimated from ultraviolet photoelectron spectroscopy (See supporting information S4). The VBM position is found to be ~3.26 eV and ~2.69 eV for $TiO_2$-NWs and N-$TiO_2$-NWs, respectively. This implies that N-doping carriers are creating sub-bands or defects above the VB of $TiO_2$.

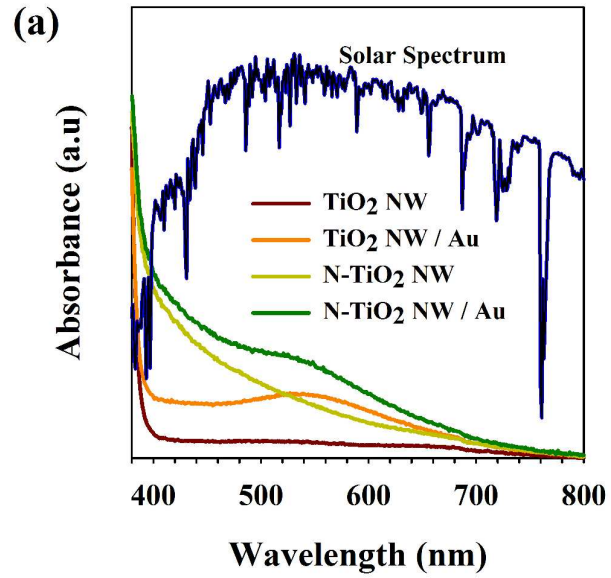


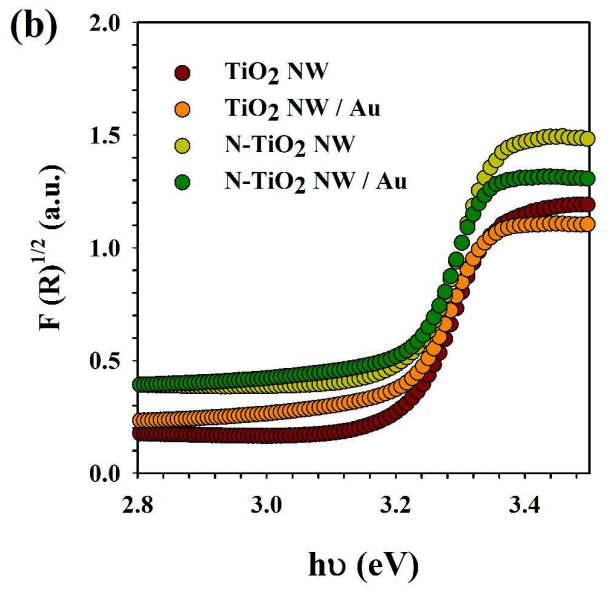


**Figure 2.** Optical absorbance spectra of different electrodes [normalized solar spectrum at AM 1.5 is compared in the Figure]; (b) band gap energy of different electrodes estimated from diffused reflectance spectra.

The strong shoulder peak around 530 nm observed (Fig. 2(a) and (b)) for Au/$TiO_2$-NWs and Au/N-$TiO_2$-NWs electrode arises from the LSPR of AuNPs. The augmented absorption at Au/N-$TiO_2$-NWs confirms its enhanced visible light activity than Au/$TiO_2$-NWs. As compared using the solar spectrum at AM 1.5 in Fig.2 (a), the major fraction of light absorbance is from visible light wavelength region than that of UV region. In this line, Au/N-$TiO_2$-NWs showed large absorbance cross section than undoped $TiO_2$. According to Du et al,[33] interaction among AuNPs afford scattering enhancement in the near-UV band, which promotes the $TiO_2$ absorption enhancement in the same region. The large amount of Au NPs decoration at N-$TiO_2$ surface (Fig.1d), further enhance the light scattering between AuNPs result high absorbance at near-UV band.

The finite-difference time-domain (FDTD) method was employed to simulate the electric field distribution at Au decorated $TiO_2$-NWs and N-$TiO_2$-NWs. Fig.3 shows the electric field (E-field) distribution in the perpendicular direction, across the AuNPs at $TiO_2$-NWs and N-$TiO_2$-NWs surface obtained from FDTD simulations. The permittivity of gold was analyzed using Lorenz-Drude dispersive model.[43]

$$\varepsilon_r(\omega) = \varepsilon_{r,\infty} + \sum_{m=0}^{5} \frac{G_m \Omega_m^2}{\omega_m^2 - \omega^2 + j\omega\Gamma_m} \qquad (1)$$

where, $\varepsilon_r(\omega)$ is the relative permittivity at infinity frequency, $G_m$ is the strength of each resonance term, $\Omega_m$ is the plasma frequency, $\omega$ and $\omega_m$ is the angular and resonant frequency, respectively, and $\Gamma_m$ is the damping factor or collision frequency.

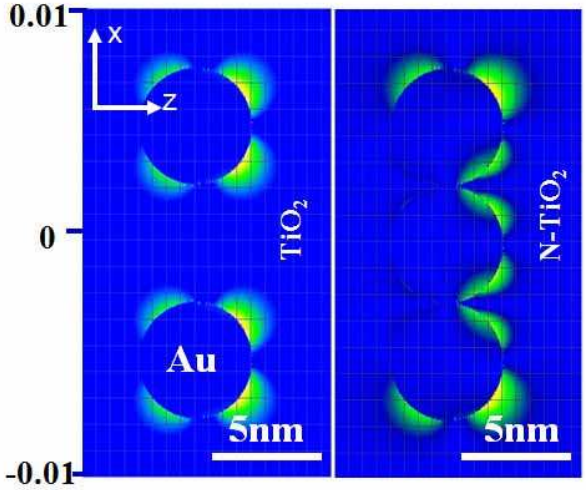


**Figure 3.** Comparison of the FDTD simulated E-field distributions of AuNPs on $TiO_2$-NWs and N-$TiO_2$-NWs. The number of AuNPs on $TiO_2$-NW (dimer with separation) and N-$TiO_2$-NW (triplet without separation) were assumed based on TEM observation (Figure 1 (d) and (e)).

From Fig.3b, E-field distribution shows strong localization of plasmon polaritons between AuNPs and N-$TiO_2$-NWs than pristine $TiO_2$-NWs, which resulted in higher optical absorbance at Au/N-$TiO_2$-NWs electrode. The intense electric field observed at Au/N-$TiO_2$-NWs surface suggests that the loading of AuNPs could markedly influence the absorbance cross section at near UV region. In close proximity at N-$TiO_2$, the hot spot electric field distribution showed ~2nm around the AuNPs surface, predominantly scattering at two adjusting Au dimers. The similar trend at Au/$TiO_2$ interfaces has been studied previously.[44-46] This enhanced electromagnetic field induced by the LSPR effect is advantageous in photocatalyst for effective e-$h^+$ charge separation at $TiO_2$/electrolyte interfaces, thus drives larger fraction of the photoinduced charge to diffuse to the catalytic surface and contribute to catalysis.[47,48]

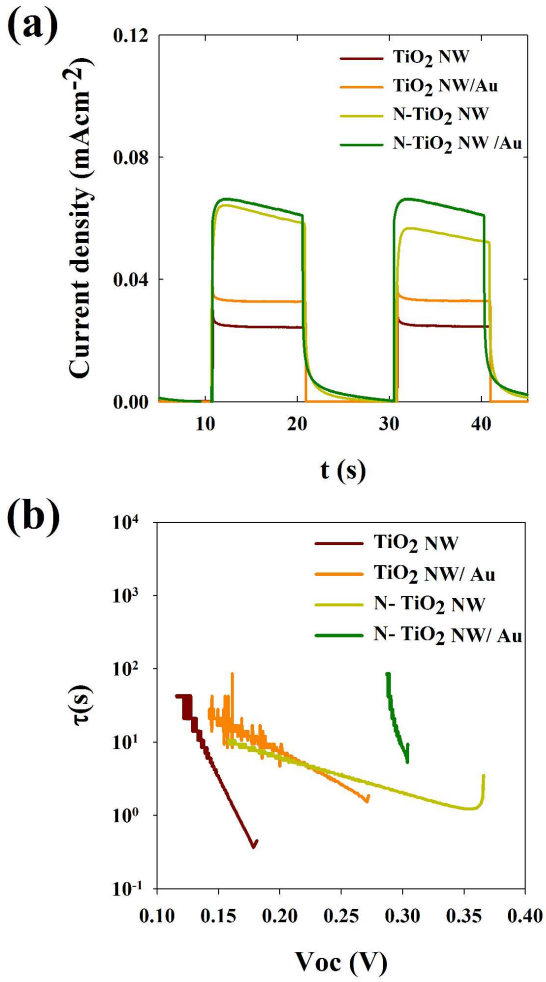


**Figure 4.** (a) *I-t* photocurrent action spectra (under 0.5M $Na_2SO_4$ aqueous electrolyte, pH=5.9), (b) open-circuit voltage decay plots measured in 0.1 M $Na_2SO_4$ electrolyte.

To get more insights into the influence of AuNPs on the photoelectrochemical performance, chronoamperometric *I–t* curves were measured (Fig. 4a) under the illumination (100 $mWcm^{-2}$) of visible light at zero bias voltage. The three electrode cell is used in this study. It clearly evince that AuNPs markedly improve the photocurrent generation from ~25 $\mu Acm^{-2}$ to ~32 $\mu Acm^{-2}$ in $TiO_2$-NWs which may be attributed to the light scattering effect. As is discussed above, the AuNPs as light scattering centres promote light harvesting photons at near UV band gap region and thus enhance the electron-hole pair generation at $TiO_2$. Further, nitrogen doping at $TiO_2$ found to enhance the photocurrent to ~60 $\mu Acm^{-2}$. This can be explained on the basis of band gap narrowing effect (Fig. 2b) enabling more visible light photons access to N-$TiO_2$.

The energy level of Au is located below the CB of $TiO_2$ and may also participate in the electrocatalytic water oxidation in addition to the Pt counter electrode which overlap with resultant photocurrent of the cell.[49] This implies that the electron pathway is feasible from $TiO_2$ CB to electrolyte through AuNPs.[50] Unprecedentedly, the Au/N-$TiO_2$-NWs show excellent photocurrent generation of about ~70 $\mu Acm^{-2}$. Such drastic improvement (~2.5 fold) in photocurrent density is ascribed to the synergistic effect of strong light scattering effect from AuNPs with the visible light driven contribution from N-doping carriers. In close proximity, photocurrent decay at light off-condition is very sharp in $TiO_2$-NWs and Au/$TiO_2$-NWs. In contrast, N-$TiO_2$-NWs showed exponential photocurrent decay trend that is ascribed to the lower recombination rate of ($e^-/h^+$) pair at oxygen vacancy sites. Further, the recombination kinetics at electrode/electrolyte interfaces and the minority carrier life time ($e^-$) of different electrodes were qualitatively studied under 0.5M $Na_2SO_4$ electrolyte using open circuit voltage decay (OCVD) techniques.[51]

The electron lifetime, $\tau_n$, was calculated using Eq.2 and the resultant $\tau_n$ *vs* $V_{oc}$ spectra is presented at Fig.4b.

$$\tau_n = (K_BT/e)[(dV_{oc})/dt]^{-1} \quad (2)$$

where, $V_{oc}$ is open circuit voltage and other parameters has their own inference.

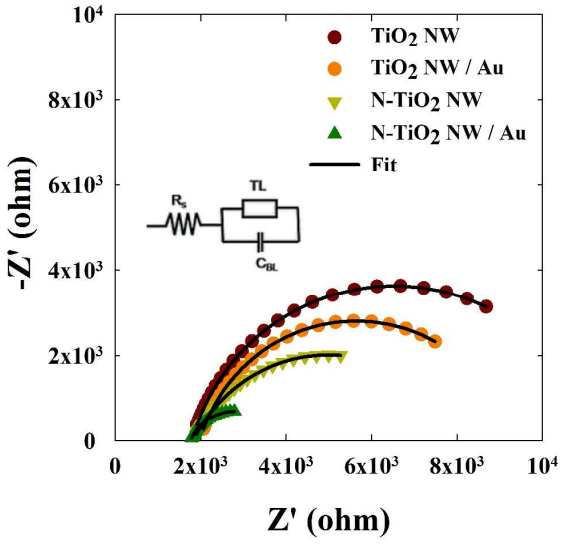


**Figure 5**. Nyquist plots measured under dark condition in 0.1 mM aqueous $Ru(bpy)_3Cl_2$.

As anticipated, Fig.4b clearly supports that AuNPs has

markedly improved the electron life time of $TiO_2$-NWs.[33] Further, $\tau_n$ is drastically promoted under N-doping compared to pristine $TiO_2$-NWs and Au/$TiO_2$-NWs electrodes. The reaction kinetics and rate of photocatalytic dye degradation process greatly depends on $e^-$ and $h^+$ charge transfer through solid−solid interface and/or solid−liquid interface. Hence, the feasibility of interfacial charge transfer at electrode/electrolyte interface was evaluated using electrochemical impedance spectra (EIS). Fig.5 shows the Nyquist plots and the excellent theoretical fitting generated using the equivalent circuit model. 0.1 mM aqueous $Ru(bpy)_3Cl_2$ was used as the electrolyte. The charge transfer resistance ($R_{ct}$) at electrode/electrolyte interfaces at $TiO_2$-NWs electrode is ~9573 Ω and is substantially reduced to ~7363 Ω at Au/$TiO_2$-NWs, due to the formation of schottky junction that promotes the electron transfer at electrode/electrolyte interfaces. Further, the $R_{ct}$ is reduced to ~6226 Ω upon N doping, owing to the hindered recombination pathways at N-$TiO_2$-NWs as discussed previously. Interestingly, a drastically decreased $R_{ct}$ is observed at Au/N-$TiO_2$-NWs electrode (~2087Ω), which is ~4 fold lesser than that observed at $TiO_2$-NWs. The drastic reduction of $R_{ct}$ at electrode/electrolyte interface causes effective space charge layer formation with high $C_\mu$=79.9×10$^{-6}$ F in this electrode. The larger $C\mu$ at Au/N-$TiO_2$-NWs electrode than $TiO_2$-NWs ($C_\mu$=4.1×10$^{-6}$ F) indicates the high feasibility of charge transfer from electrode to electrolyte with reduced recombination which in-turn could facilitate the PC dye degradation performance. The prolonged decay at N-$TiO_2$-NWs validated the high ($e^-/h^+$) pair charge separation rate due to the blocked recombination pathways (oxygen vacancies) in $TiO_2$.[20] High carrier lifetime along with the simultaneous improvement in reducing oxygen vacancies at Au/N-$TiO_2$-NWs is responsible for high photocurrent observed in these electrodes (Fig.4a).

The photocatalytic efficiencies of different electrodes were investigated through measuring the decolourization of methyl orange (MO) under visible light irradiation (λ>400 nm). In the absence of catalyst, MO is stable under visible light irradiation and after introducing the pure and modified $TiO_2$ nanostructured electrodes the PC degradation rate of MO increased monotonically as a function of the electrode performance. The photocatalytic efficiencies of different electrodes were investigated through measuring the decolourization of methyl orange (MO) under visible light irradiation (λ>400 nm). It is apparent from Fig.6 that 92% of MO was degraded at Au/N-$TiO_2$ NWs within 3 hrs of visible light irradiation, whereas only 73% decolourization was noticed in the absence of AuNPs. This is ascribed to the existence of strong LSPR between AuNPs and N-$TiO_2$-NWs. The $TiO_2$-NWs and Au/$TiO_2$-NWs exhibit only 44% of decolourization under identical conditions. The catalytic performance of pristine $TiO_2$-NWs under visible light irradiation is due to the one-dimensional structure of $TiO_2$-NWs.[30] It is worth noticing that the Au/$TiO_2$-NWs show no change in photocatalytic efficiency despite the presence of AuNPs. This could be due to weak interaction between AuNPs and $TiO_2$-NWs. The degradation of MO follows the pseudo first order kinetics and the rate constant for Au/N-$TiO_2$-NWs (1.1×10$^{-2}$ min) is ~4 folds higher than $TiO_2$-NWs (2.9×10$^{-3}$ min$^{-1}$) and ~2 folds higher than N-$TiO_2$-NWs (7.0×10$^{-3}$ min$^{-1}$).

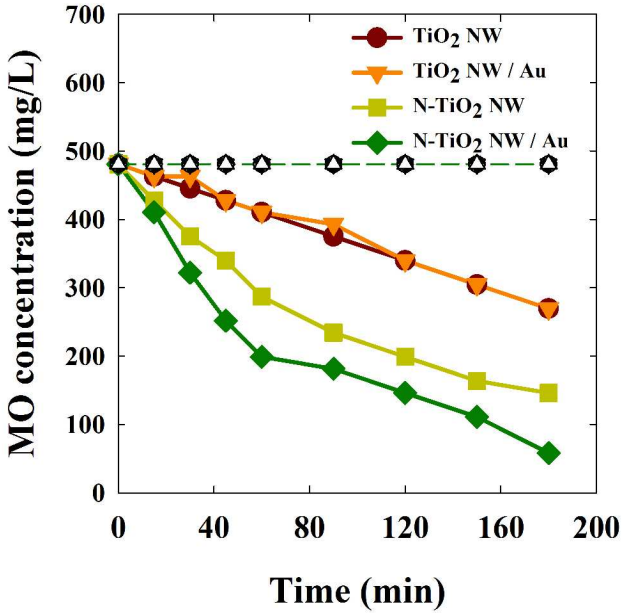


**Figure 6.** photocatalytic degradation of MO at various photoelectrodes for different time course [symbols 'Δ' and '●' represents the experiments under dark condition and absence of photocatalyst, respectively].

The mechanism of enhanced photocatalytic degradation of MO is illustrated in Scheme 1, which can be explained as follows: Under visible light irradiation, photogenerated electron-hole pairs are formed in AuNPs due to surface plasmon resonance. The photoexcited electrons at N-$TiO_2$ conduction band electrons scavenge the oxygen molecules and form highly reactive superoxide radicals ($O_2^{\bullet-}$); then on protonation yields $HOO^\bullet$ radicals. Owing to the formation of schottky barrier at Au/$TiO_2$ interface, part of the photoelectrons is transferred from CB of $TiO_2$ to AuNPs. These injected electrons also forming highly reactive superoxide radicals ($O_2^{\bullet-}$). The resultant $HOO^\bullet$ radicals combines with the trapped electrons forming $H_2O_2$, finally forming $OH^\bullet$.[52] These active species ($OH^\bullet$) results in the degradation and mineralization of MO. Meanwhile, the holes in $TiO_2$ VB scavenge the surface adsorbed water to form highly reactive hydroxyl radicals ($OH^\bullet$). All these radicals are highly active towards degradation of MO resulting in enhanced photocatalytic degradation rates upon visible light irradiation. Similarly, the holes at the valence band of N-$TiO_2$ effectively reach water forming hydroxyl radicals ($OH^\bullet$). The collective generation of hydroxyl radicals by N-$TiO_2$-NWs and additional superoxide radicals at AuNPs, undoubtedly, enhances the photocatalytic dye degradation performance. It is presumed that the increase in the amount of AuNPs loading could further enhance the photocatalytic dye degradation performance. However, the maximum photocatalytic activity might not be achieved at the highest loading since there exist a trade-off between the improved photocatalytic activities owing to the enhanced charge separation and decreased light absorption by the host photocatalyst due to increased AuNPs loading. One of the critical issues on quantifying the PC performance through decolourization of dye molecules is physical adsorption of MO

dye molecules on Au/N-$TiO_2$ electrode (dye sensitization).[53, 54] However the quantity of dye molecules physically adsorbed onto Au/N-$TiO_2$ electrode is extremely lesser than that of photocatalytically bleaching dye molecules (dye loading test after experiments is carried out using 0.1 M NaOH solution, not presented in the manuscript). It is anticipated that the analysis of photocatalytic decomposition of colourless substances could be a better choice to preclude the undesirable issues involved in quantifying the PC performance.

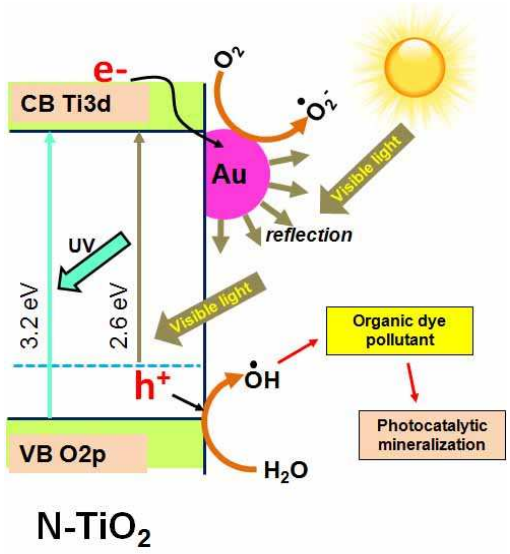


**Scheme 1.** Schematic mechanism of organic dye pollutant degradation on Au NPs decorated N-$TiO_2$ nanowire.

## Conclusions

Enhanced visible light activity of high surface area, vertically grown $TiO_2$-NWs was demonstrated using N-doping as well as assembling AuNPs using a simple one-step process. The subsequent effect of (a) high charge-pair separation, (b) extended visible light absorption driven by N-doping and (c) light scattering effect from AuNPs, fostered Au/N-$TiO_2$-NWs as futuristic electrodes with superior photocatalytic activity toward organic dye pollutant removal. Our significant findings on enhancing the photocatalytic activity of $TiO_2$ through N-doping and AuNPs immobilization render Au/N-$TiO_2$-NWs electrode, a promising photoanode for collecting the photoelectrons remotely for simultaneous hydrogen generation or $CO_2$ reduction.

## Experimental Section

### Photoelectrode fabrication

All materials were purchased from Sigma-Aldrich and were used as received. The $TiO_2$-NWs array (~4μm thickness) is directly prepared on FTO substrate using pre-coated ZnO-NWs templates. Detailed description on the preparation of $TiO_2$-NWs, N-$TiO_2$-NWs and DMAP-protected AuNPs were described in our earlier reports.[42, 55, 56] Au/$TiO_2$-NWs and Au/N-$TiO_2$-NWs were prepared by simply dipping the $TiO_2$-NWs and N-$TiO_2$-NWs electrodes in aqueous solution containing $3.3\times10^6$ M of DMAP-protected AuNPs for 1 min and the electrodes were successively washed with water thrice to remove the weakly adsorbed AuNPs. The AuNPs get instantaneously adsorbed onto the NWs *via* electrostatic attraction between positively charged AuNPs and negatively (due to the existence of OH groups at the surface) charged $TiO_2$ NWs surface.

### Characterization

The morphology of electrodes was observed using a field emission scanning electron microscope (FE-SEM, JEOL JSM-7600F) and field emission transmission electron microscope (FE-TEM, JEOL JEM-2100F). The optical absorption and diffused reflectance spectra of the electrodes were recorded in the range of 350–900 nm using a V670 JASCO UV-Vis spectrophotometer. The electrochemical impedance (EIS) and photocurrent *vs* time (*I-t*) were recorded using three electrode electrochemical cells with a FRA-equipped PGSTAT-30 from Autolab. The EIS measurements were carried out under dark condition with applying a 20 mV AC signal and scanning in the frequency range between 400 kHz and 0.1 Hz at 0.5V applied voltage.[57] The (*I-t*) measurements were performed at zero applied potential. The aqueous 0.5M $Na_2SO_4$ electrolyte was used as electrolyte. The photocurrent measurements were recorded in 1 sun condition ($100mWcm^{-2}$) with the visible light irradiation using a solar simulator with a 300 W xenon arc-lamp (Newport). The light intensity was calibrated using a silicon solar cell (PV measurements, Inc.)The permittivity of gold was analyzed using Lorenz-Drude dispersive model with the aid of finite difference time domain method (FDTD) simulation (Optiwave software package).[58]

### Photocatalytic activity measurements

A compact Xe light source with an emission of $\lambda > 350$ nm was used (ASAHI Spectra Co., Ltd, Japan, model HAL 320) as a source for visible light radiation. The light intensity was adjusted to 75 $mWcm^{-2}$ using Si-photodiodes (Asahai Spectra, model CS20). The distance between the visible light source and the photoelectrode was fixed at 5 cm in the photoelectrochemical reactor. Methyl orange (MO) dye was the model pollutant used to evaluate the PC performance of the photoelectrodes. The initial concentration of MO was 500 mg $L^{-1}$. The volume of MO used is 10 mL. A UV-Vis spectrophotometer (V670 JASCO) was used to analyze the concentration of MO during the course of photodegradation.

## Acknowledgements

This work was supported by the Global Research Laboratory (GRL) Program (K20704000003TA050000310) and Korea through the National Research Foundation of Korea (NRF) funded by the Ministry of Science. This research was also supported by the Korea Center for Artificial Photosynthesis (KCAP, NRF-2012-M1A2A2671834), the Priority Research Centers Program (2011-0031407). One of the authors P.S. acknowledges the financial support from Japan Society for the Promotion of Science (JSPS) for providing a Postdoctoral Research Fellowship.

## Notes and references

[a] *Department of Energy Engineering, Hanyang University, Seoul 133-791, Korea. E-mail:upaik@hanyang.ac.kr; kangys@hanyang.ac.kr*
[b] *Department of Materials Science and Engineering, Hanyang University, Seoul 133-791, Korea.*
[c] *Photocatalysis International Research Center, Tokyo University of Science, 2641 Yamazaki, Noda, Chiba 278-8510, Japan.*
[d] *Semiconductor Physics Research Center, School of Semiconductor and Chemical Engineering, Chonbuk National University, Jeonju 561-756 (Korea)*

† Electronic Supplementary Information (ESI) available: See DOI: 10.1039/b000000x/

‡ These authors contributed equally to this work.

1. A. Fujishima and K. Honda, *Nature*, 1972, **238**, 37-38.
2. J. R. Bolton, *Science*, 1978, **202**, 705-711.
3. A. Fujishima, X. Zhang and D. A. Tryk, *International Journal of Hydrogen Energy*, 2007, **32**, 2664-2672.
4. A. Kudo and Y. Miseki, *Chemical Society Reviews*, 2009, **38**, 253-278.
5. G.-J. Chee, Y. Nomura, K. Ikebukuro and I. Karube, *Biosensors and Bioelectronics*, 2005, **21**, 67-73.
6. A. Devadoss, P. Sudhagar, S. Das, S. Y. Lee, C. Terashima, K. Nakata, A. Fujishima, W. Choi, Y. S. Kang and U. Paik, *ACS Applied Materials & Interfaces*, 2014.
7. I. Tooru, F. Akira, K. Satoshi and H. Kenichi, *Nature*, 1979, **277**, 637-638.
8. W. Rong, H. Kazuhito, F. Akira, C. Makota, K. Eiichi, K. Atsushi, S. Mitsuhide and W. Toshiya, *Nature*, 1997, **388**, 431-432.
9. E. Stathatos, T. Petrova and P. Lianos, *Langmuir*, 2001, **17**, 5025-5030.
10. J. Kim, D. Monllor-Satoca and W. Choi, *Energy & Environmental Science*, 2012, **5**, 7647-7656.
11. P. Lianos, *Journal of Hazardous Materials*, 2011, **185**, 575-590.
12. J. Choi, P. Sudhagar, P. Lakshmipathiraj, J. W. Lee, A. Devadoss, S. Lee, T. Song, S. Hong, S. Eito, C. Terashima, T. H. Han, J. K. Kang, A. Fujishima, Y. S. Kang and U. Paik, *RSC Advances*, 2014, **4**, 11750-11757.
13. P. Lianos, *Journal of Hazardous Materials*, 2011, **185**, 575-590.
14. S. George, S. Pokhrel, Z. Ji, B. L. Henderson, T. Xia, L. Li, J. I. Zink, A. E. Nel and L. Mädler, *Journal of the American Chemical Society*, 2011, **133**, 11270-11278.
15. Z. Yao, F. Jia, S. Tian, C. Li, Z. Jiang and X. Bai, *ACS Applied Materials & Interfaces*, 2010, **2**, 2617-2622.
16. H. Jie, H. Park, K. B. Lee, H. J. Chang, J. P. Ahn and J. K. Park, *Surf Interface Anal*, 2012, **44**, 1449-1452.
17. H. Zhu, J. Tao and X. Dong, *The Journal of Physical Chemistry C*, 2010, **114**, 2873-2879.
18. H. Irie, K. Kamiya, T. Shibanuma, S. Miura, D. A. Tryk, T. Yokoyama and K. Hashimoto, *The Journal of Physical Chemistry C*, 2009, **113**, 10761-10766.
19. M. Liu, X. Qiu, M. Miyauchi and K. Hashimoto, *Journal of the American Chemical Society*, 2013, **135**, 10064-10072.
20. P. Sudhagar, K. Asokan, E. Ito and Y. S. Kang, *Nanoscale*, 2012, **4**, 2416-2422.
21. Q. Sun, J. Zhang, P. Q. Wang, J. Zheng, X. N. Zhang, Y. Z. Cui, J. W. Feng and Y. J. Zhu, *J Renew Sustain Ener*, 2012, **4**.
22. J. H. Park, S. Kim and A. J. Bard, *Nano Letters*, 2005, **6**, 24-28.
23. A. Naldoni, M. Allieta, S. Santangelo, M. Marelli, F. Fabbri, S. Cappelli, C. L. Bianchi, R. Psaro and V. Dal Santo, *Journal of the American Chemical Society*, 2012, **134**, 7600-7603.
24. X. Chen, L. Liu, P. Y. Yu and S. S. Mao, *Science*, 2011, **331**, 746-750.
25. P. Sudhagar, V. Gonzalez-Pedro, I. Mora-Sero, F. Fabregat-Santiago, J. Bisquert and Y. S. Kang, *Journal of Materials Chemistry*, 2012, **22**, 14228-14235.
26. P. Sudhagar, T. Song, D. H. Lee, I. Mora-Seró, J. Bisquert, M. Laudenslager, W. M. Sigmund, W. I. Park, U. Paik and Y. S. Kang, *The Journal of Physical Chemistry Letters*, 2011, **2**, 1984-1990.
27. P. Christopher, H. Xin, A. Marimuthu and S. Linic, *Nature Materials*, 2012, **11**, 1044-1050.
28. A. A. Harry and P. Albert, *Nature Materials*, 2010, **9**, 205-213.
29. I. Paramasivam, J. M. Macak and P. Schmuki, *Electrochemistry Communications*, 2008, **10**, 71-75.
30. L. Xiang, X. Zhao, C. Shang and J. Yin, *Journal of Colloid and Interface Science*, 2013, **403**, 22-28.
31. I. M. Arabatzis, T. Stergiopoulos, D. Andreeva, S. Kitova, S. G. Neophytides and P. Falaras, *Journal of Catalysis*, 2003, **220**, 127-135.
32. A. Primo, A. Corma and H. Garcia, *Physical Chemistry Chemical Physics*, 2011, **13**, 886-910.
33. L. Du, A. Furube, K. Yamamoto, K. Hara, R. Katoh and M. Tachiya, *The Journal of Physical Chemistry C*, 2009, **113**, 6454-6462.
34. S.-Y. Du and Z.-Y. Li, *Opt. Lett.*, 2010, **35**, 3402-3404.
35. Z. Zhang, L. Zhang, M. N. Hedhili, H. Zhang and P. Wang, *Nano Letters*, 2013, **13**, 14-20.
36. D. B. Ingram and S. Linic, *Journal of the American Chemical Society*, 2011, **133**, 5202-5205.
37. S. Oros-Ruiz, R. Zanella and B. Prado, *Journal of Hazardous Materials*, 2013.
38. E. Pedrueza, J. L. Valdés, V. Chirvony, R. Abargues, J. Hernández-Saz, M. Herrera, S. I. Molina and J. P. Martínez-Pastor, *Advanced Functional Materials*, 2011, **21**, 3502-3507.
39. M. Miyauchi, A. Ikezawa, H. Tobimatsu, H. Irie and K. Hashimoto, *Physical Chemistry Chemical Physics*, 2004, **6**, 865-870.
40. J. Graciani, A. Nambu, J. Evans, J. A. Rodriguez and J. F. Sanz, *Journal of the American Chemical Society*, 2008, **130**, 12056-12063.
41. H. Irie, Y. Watanabe and K. Hashimoto, *Journal of Physical Chemistry B*, 2003, **107**, 5483-5486.
42. P. Rodenas, T. Song, P. Sudhagar, G. Marzari, H. Han, L. Badia-Bou, S. Gimenez, F. Fabregat-Santiago, I. Mora-Sero, J. Bisquert, U. Paik and Y. S. Kang, *Advanced Energy Materials*, 2013, **3**, 176-182.
43. A. D. Rakić, A. B. Djurišić, J. M. Elazar and M. L. Majewski, *Applied Optics*, 1998, **37**, 5271-5283.
44. Z. Liu, W. Hou, P. Pavaskar, M. Aykol and S. B. Cronin,

*Nano Letters*, 2011, **11**, 1111-1116.
45. Z. Zhan, J. An, H. Zhang, R. V. Hansen and L. Zheng, *ACS Applied Materials & Interfaces*, 2014, **6**, 1139-1144.
46. Z. Bian, T. Tachikawa, P. Zhang, M. Fujitsuka and T. Majima, *Journal of the American Chemical Society*, 2013, **136**, 458-465.
47. Y.-C. Pu, G. Wang, K.-D. Chang, Y. Ling, Y.-K. Lin, B. C. Fitzmorris, C.-M. Liu, X. Lu, Y. Tong, J. Z. Zhang, Y.-J. Hsu and Y. Li, *Nano Letters*, 2013, **13**, 3817-3823.
48. J. Qiu, G. Zeng, P. Pavaskar, Z. Li and S. B. Cronin, *Physical Chemistry Chemical Physics*, 2014, **16**, 3115-3121.
49. W. Hou, W. H. Hung, P. Pavaskar, A. Goeppert, M. Aykol and S. B. Cronin, *ACS Catalysis*, 2011, **1**, 929-936.
50. X. Zhang, Y. L. Chen, R. S. Liu and D. P. Tsai, *Reports on Progress in Physics*, 2013, **76**.
51. A. Zaban, M. Greenshtein and J. Bisquert, *ChemPhysChem*, 2003, **4**, 859-864.
52. X. Z. Li and F. B. Li, *Environmental Science and Technology*, 2001, **35**, 2381-2387.
53. M. Mrowetz, W. Balcerski, A. J. Colussi and M. R. Hoffmann, *The Journal of Physical Chemistry B*, 2004, **108**, 17269-17273.
54. X. Yan, T. Ohno, K. Nishijima, R. Abe and B. Ohtani, *Chemical Physics Letters*, 2006, **429**, 606-610.
55. H. Han, T. Song, J.-Y. Bae, L. F. Nazar, H. Kim and U. Paik, *Energy & Environmental Science*, 2011, **4**, 4532-4536.
56. A. Devadoss, C. Dickinson, T. E. Keyes and R. J. Forster, *Analytical Chemistry*, 2011, **83**, 2383-2387.
57. P. Sudhagar, V. González-Pedro, I. Mora-Seró, F. Fabregat-Santiago, J. Bisquert and Y. S. Kang, *Journal of Materials Chemistry*, 2012, **22**, 14228-14235.
58. A. D. Rakic, A. B. Djuri?ic, J. M. Elazar and M. L. Majewski, *Appl. Opt.*, 1998, **37**, 5271-5283.

**Graphical abstract**

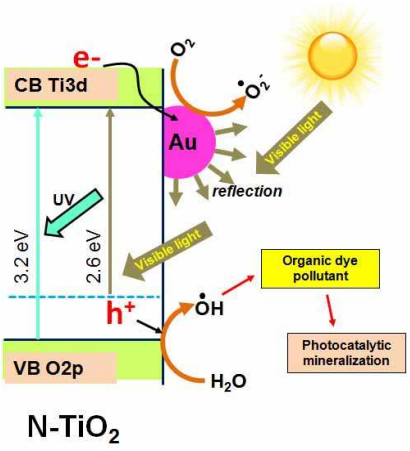


Maximizing the Au nanoparticle decoration on $TiO_2$ nanowire through nitrogen doping for simultaneous enhancement in visible light scattering and electron-hole charge separation